

On the Secrecy Enhancement of an Integrated Ground-Aerial Network with a Hybrid FSO/THz Feeder Link

Elmehdi Illi, *Member, IEEE*, and Marwa Qaraqe, *Senior Member, IEEE*

Abstract—High altitude platforms (HAPs)-aided terrestrial-aerial communication technology based on free-space optical (FSO) and Terahertz (THz) feeder links has been attracting notable interest recently due to its great potential in reaching a higher data rate and connectivity. Nonetheless, the presence of harsh vertical propagation environments and potential aerial eavesdroppers are two of the main challenges limiting the reliability and security of such a technology. In this work, a secrecy-enhancing scheme for HAP-aided ground-aerial communication is proposed. The considered network consists of HAP-assisted communication between a ground station and a legitimate user under the threat of an aerial and ground eavesdropper. Thus, the proposed scheme leverages (i) HAP diversity by exploiting the presence of multiple flying HAPs and (ii) the use of a hybrid FSO/THz transmission scheme to offer better resilience against eavesdropping attacks. An analytical secrecy outage probability (SOP) expression is derived for the scheme in consideration. Results manifest the notable gain in security of the proposed scheme with respect to both (i) the single-HAP and (ii) THz feeder-based benchmark ones, where the proposed scheme's SOP is decreased by four orders of magnitude using 4 HAPs with respect to the first benchmark scheme, while a 5-dB secrecy gain is manifested with respect to the second benchmark one.

Index Terms—Atmospheric attenuation, high-altitude platforms, free-space optics, physical layer security, Terahertz communication, pointing errors.

I. INTRODUCTION

Throughout the past few years, there has been an increasing interest in exploiting the aerial interface, composed of unmanned aircraft, high-altitude platforms (HAPs), and satellites, for extending the area coverage of several underserved zones over the earth and significantly increasing the peak data rate [1]. HAPs and satellites can broaden communication coverage and boost data rates through multi-beam transmissions and by leveraging very high-throughput backhaul/feeder links from an earth station. In this optic, HAPs manifested several benefits compared to conventional low-earth orbit (LEO) satellites, essentially its shorter signal round-trip time compared to their LEO counterpart due to the shorter distance to the earth surfaces, i.e., placed in the stratosphere (17-50 Km), hence providing a low communication latency [2].

From another front, the adoption of the THz and FSO transmissions as a backhaul feeder link for terrestrial-aerial/satellite transmissions has been among the advocated solutions to cater to the high data rate needs. Such technologies can

solve the spectrum saturation issue in the radio frequency (RF) spectrum in the Ku and Ka bands [2], [3]. FSO is based on transmitting conical-shaped optical beams in the infrared (IR)/near IR or visible light spectrum. Its immunity to interference, security, high amount of bandwidth, and low implementation cost make FSO feeder links a viable solution for the continuous needs in bandwidth. On the other hand, THz technology is based on the utilization of the 0.1 THz-10 THz RF spectrum for transmitting directive RF beams [4]. To this end, THz technology can offer at least an order of magnitude of bandwidth gain compared to its mmWave counterpart. However, despite the aforementioned features, the two technologies suffer from several common impairments, such as beam wandering, atmospheric turbulence-induced fading, and, essentially, beam pointing errors due to the transceivers' vibration/movement. In addition to this, it has been shown that FSO suffers heavily from meteorological conditions, such as the presence of fog, heavy rain, and clouds, whereas THz manifests better resilience against severe weather. It is worth mentioning that the presence of molecular absorption is an additional impairment affecting the THz communication's performance, while the FSO transmission is less affected by it.

The physical layer security (PLS) paradigm has been attracting the wireless community in the past years. PLS' objective is to ensure secure keyless transmission, from either a confidentiality or authentication point of view, relying solely on the physical layer parameters, e.g., fading, antenna diversity, and precoding. Confidentiality-based PLS relies on maximizing/enhancing the secrecy capacity (SC) metric to counter eavesdropping attacks, which can guarantee a higher transmission rate as well as a target decoding failure at eavesdroppers. From FSO and THz communications point of view, in spite of their high beam directivity, exhibiting "by nature" a secure transmission, THz and optical beams are of divergent nature at higher transmission distances. Precisely, the beam spot size at an aerial receiver in the stratosphere can reach the order of tens-hundreds of meters, which puts it under a continuous threat of malicious aircraft/unmanned aerial vehicles (UAVs) that can be located within the beam divergence area and eavesdrop on the ground-space/satellite feeder link [5], [6]. Therefore, securing the feeder link in hybrid terrestrial-aerial/satellite links is crucial.

E. Illi and M. Qaraqe are with the College of Science and Engineering, Hamad Bin Khalifa University, Qatar Foundation, Doha, Qatar. (e-mails: elmehdi.illi@ieee.org, mqaraqe@hbku.edu.qa).

A. Related Work

Concerning the literature on FSO-based terrestrial-aerial/satellite networks, several works inspected its performance in terms of bit error and outage probabilities and link margin, as detailed in [7]–[9]. In addition to this, the authors of [10] explored the potential of THz communication in airplane-satellite links, whereby a holistic channel modeling encompassing the various propagation attenuation phenomena and a performance evaluation of the system were provided. On the other hand, several techniques have been proposed to enhance the performance of ground-aerial/satellite networks. For instance, the authors in [11] proposed the incorporation of site diversity by using multiple ground stations to counter the high attenuation of ground-satellite FSO links. Furthermore, in [12], [13], another approach was proposed to enhance the reliability performance of hybrid terrestrial-aerial/satellite networks by adopting a hybrid RF/FSO transmission, where the system switches to the RF Ka-band signals whenever the received FSO signal power falls below a threshold limit. Furthermore, in [14], a HAPs diversity scheme was proposed to increase the reliability of downlink satellite-HAP-earth networks by selecting the best relaying HAP in terms of the instantaneous signal-to-noise ratio (SNR).

From another front, some research works inspected the secrecy of FSO- and THz-based terrestrial-aerial/satellite networks. For instance, the secrecy of a dual-hop terrestrial-satellite network was analyzed in [3] with an FSO feeder link and under the presence of an eavesdropper in each of the two hops, i.e., uplink ground-satellite and downlink satellite-ground. In order to increase the secrecy of the considered network, both optical aperture diversity and RF beams precoding were considered. Also, Ma et al. tackled in [15] the secrecy evaluation of a mixed RF-FSO uplink terrestrial-satellite connection assisted by a relay UAV. In addition, the authors of [16] analyzed the security level of a satellite- and HAP-based network under two communication scenarios, namely the satellite-to-HAP and HAP-to-ground under eavesdropping attacks. The same authors inspected in [17] the secrecy of a satellite-ground communication system assisted by a HAP as a relay, where an eavesdropper attempts to compromise the second hop operating with RF Ka-band. In [18], the security of an RF-based reconfigurable intelligent surface (RIS)-and UAV-aided satellite-ground communication was analyzed in the presence of multiple ground eavesdroppers. The work of Ben Yahia et al. in [19] aimed to inspect the security of an FSO-based satellite-HAP network when a malicious spacecraft attempts to overhear the legitimate signal from the divergent optical beam. The same authors elaborated an extension of the aforementioned work in [20], where the analysis of secrecy considered FSO-based satellite-HAP, uplink ground-HAP, and downlink HAP-ground networks in the presence of a HAP eavesdropper. In [21], a cognitive radio-based terrestrial-satellite network with an optical feeder link was quantified in terms of the key system parameters. It is worth highlighting notable existing works that quantified the secrecy level of terrestrial FSO communication systems under different eavesdropping situations and positions, such as in [5], [6].

Lastly, from the THz-based vertical networks' point of view, the work in [22] provided a thorough secrecy investigation of a THz-based downlink satellite-ground communication aided by a HAP. A RIS is mounted onboard the HAP to act as a passive relay and beamsteer the THz beam towards a ground user, under the presence of an eavesdropper in its vicinity.

B. Motivation

It has been established from the above-discussed literature work that the reliability performance of FSO- and THz-based hybrid terrestrial-aerial/satellite networks is heavily impacted by atmospheric attenuation, turbulence, and beam misalignment (pointing errors). The proposed reliability enhancing techniques, such as HAP/site diversity and hybrid RF/FSO transmission, have been established to fulfill a higher reliability target based on the received SNR as a metric [11]–[14]. On the other hand, from a network secrecy point of view, most prior secrecy investigations considered eavesdropping threats solely on the RF side of the network, i.e., generally in the fronthaul (radio access) satellite/HAP-to-earth station (user) links. Also, the work in [16], [19], [20], [22] showed that the system's secrecy can exhibit some weakness in several scenarios. Essentially, the FSO, THz, and RF links' impairments in such vertical links significantly affect their respective secrecy. Therefore, it is of paramount importance to design secrecy-enhancing schemes for terrestrial-aerial/satellite networks to fulfill better data reliability (higher SNR levels) and also higher resilience against eavesdropping attacks from potential aerial eavesdroppers.

Motivated by the above, the current work aims to propose a novel PLS scheme for hybrid terrestrial-aerial networks by exploiting both HAPs diversity alongside a hybrid FSO/THz-feeder link transmission. The considered network consists of a HAP-aided communication between a ground station (GS) and a ground user, whereby the GS-HAP communication operates mainly over an FSO link due to its very high data rates, whereas the HAP decodes and forwards the received signal to the ground user. Under the potential presence of an eavesdropping HAP and a ground eavesdropper aiming to compromise both transmission hops, the proposed scheme aims at the exploitation of multiple available flying HAPs within the reach of the legitimate transmit ground station (GS) to select the one maximizing its secrecy performance under the presence of several aerial eavesdroppers and a single terrestrial one. In addition to this, the proposed scheme relies on a hybrid FSO/THz GS-HAPs feeder link, whereby THz transmission is activated as a backup link whenever the FSO transmission fails in fulfilling a target secrecy level. The use of THz as a backup link is expected to enhance the secrecy performance of the system further, in addition to HAP diversity, due to its resilience to propagation phenomena compared to its FSO counterpart. The current work exhibits the main differences with respect to the aforementioned previous works, where in [11]–[14], the performance of the considered networks was analyzed from reliability's point of view and not analyzing the secrecy considering either HAPs diversity [14] or hybrid RF/FSO links [12], [13], while in [3], [15]–[20], [22], [23],

the secrecy performance was inspected by considering FSO-feeder links and a single relay/HAP/satellite. To the best of our knowledge, the current work is the first to propose the use of HAPs diversity and hybrid FSO/THz transmission for the secrecy enhancement of HAP-aided terrestrial-aerial networks.

C. Contributions

The main contributions of the current work can be summarized as follows:

- A novel secrecy-enhancing scheme is proposed by harnessing the benefits of HAPs diversity and hybrid THz/FSO transmission.
- A novel mathematical framework for evaluating the network's secrecy outage probability (SOP) metric is derived, encompassing key system parameters.
- Several analytical observations are provided to demonstrate analytically the effect of some system parameters.
- Extensive numerical simulations are conducted to analyze the effect of key system parameters on the system's secrecy performance.

The rest of this paper is organized as follows: Section II presents the considered system and channel model, while Section III provides useful statistical functions for the secrecy evaluation. In Section IV, the proposed scheme is detailed, and its secrecy performance is derived. Section V is dedicated to showing illustrative numerical results for the system's secrecy. Lastly, Section VI concludes the paper.

II. SYSTEM MODEL

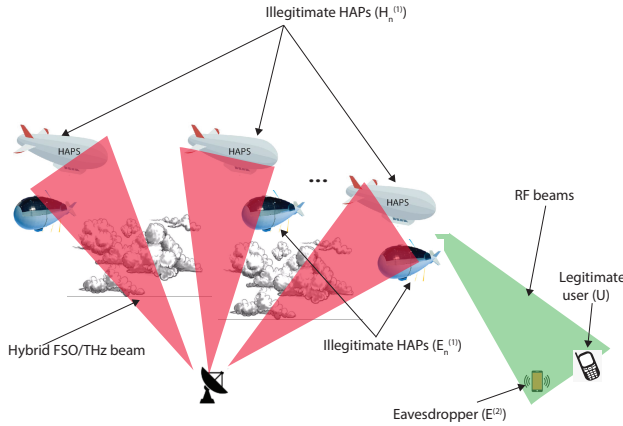


Fig. 1: System model

The transmission from the GS at the earth to an end-user is carried out through the help of N HAPs $\{H_n\}_{n=1,\dots,N}$ acting as relays, as shown in Fig. 1. FSO beams convey the transmit data symbols of the ground user over a turbulent uplink vertical channel impaired by atmospheric turbulence, scattering caused by particles, free-space path loss, and the potential presence of clouds, rain, or fog. In addition to this, the beam misalignment between the ground station and each relay HAP causes inevitable pointing errors. Furthermore,

multiple eavesdropping HAPs $\{E_n^{(i)}\}_{n=1,\dots,N}$ are targeting the legitimate information beams, where each malicious HAP is located at the vicinity of a legitimate one, precisely in the optical beam divergence area, to decode the legitimate signal. Due to the presence of the aforementioned impairments, the FSO link might become unreliable at some transmission slots and manifests a very high power loss. To this end, a backup THz link is adopted to ensure a backhaul communication between the GS and the HAP in the case of the FSO link's severe attenuation. The GS selects a HAP among the N HAPs according to the highest secrecy level, which will be detailed in the next section. Afterward, the selected HAP decodes the received information signal over either the THz or FSO link, regenerates it, and forwards it to a ground user U using an RF link operating over the Ka-band. It is assumed that the second hop's communication is under the threat of a malicious ground eavesdropper $E^{(2)}$ that targets the illegitimate interception of the RF beam.

1) *FSO Link*: The optical wireless transmission between the earth and the flying HAPs is established using either intensity modulation with direct detection (IM/DD) or coherent heterodyne detection (CHD) one. While the former is established by modulating the information using the light intensity of the optical signal, the latter technique conveys the information symbols using the amplitude (i.e., intensity), phase, or frequency. In addition to this, each eavesdropper is assumed to capture a portion ρ_E of the optical beam's power that was not captured by the corresponding legitimate HAP, as proposed in [5]. Without loss of generality, it is assumed that the optical power is shared between the legitimate and illegitimate HAPs such that $\rho_{H_n} = 1 - \rho_{E_n}$, with ρ_{H_n} indicating the portion of power captured by the n th legitimate HAP H_n . To this end, the received optical signal at the n th legitimate/illegitimate HAP, using both aforementioned techniques can be expressed as follows [3]

$$y_{X_n}^{(\text{FSO})} = (\eta \rho_X I_{S X_n})^{\frac{r}{2}} x + w_{X_n}, X \in \{H, E^{(1)}\} \quad (1)$$

where η is the electrical-to-optical conversion efficiency in A/W, $I_{S X_n}$ is the received light irradiance, x is the transmit signal with an average optical power $E[x] = P_o$, $r \in \{1, 2\}$ is a detection-dependent parameter that equals 1 for CHD and 2 for the IM/DD, and w_{X_n} is the additive white Gaussian noise process (AWGN) at the receiving HAP of zero mean and variance $\sigma_{F_n}^2$. The received light irradiance generally results from three main signal attenuation phenomena, namely:

- 1) The atmospheric attenuation, denoted by $I_{S X_n}^{(l)}$, due to the scattering by air particles throughout the propagation path, rain/fog attenuation, and free-space path-loss.
- 2) The induced fading caused by atmospheric turbulence, i.e., $I_{S X_n}^{(a)}$.
- 3) The pointing errors fluctuating attenuation caused by transceivers misalignment, i.e., $I_{S X_n}^{(p)}$.

Consequently, the resulting light irradiance expression can be formulated as follows: $I_{S X_n} = I_{S X_n}^{(l)} I_{S X_n}^{(a)} I_{S X_n}^{(p)}$. The path-loss term is mainly caused by scattering loss through the small droplets in rain, fog, and clouds, and other particles in the atmosphere. In addition to this, propagation's free-space path

loss attenuates the received optical signal power. As a result, the aggregate optical attenuation can be expressed as [14], [24]–[26]

$$I_{SX_n}^{(l)} = \exp\left(-\sigma_n L_{SX_n}^{(\text{eff,cloud/fog [km]})}\right) \exp\left(-\frac{\tau_{X_n}}{\cos(\psi_{SX_n})}\right) \times 10^{-\delta_{SX_n}^{(\text{rain,FSO})} L_{SX_n}^{(\text{eff,rain})} G_S^{(\text{T,FSO})} G_{X_n}^{(\text{R,FSO})} \left(\frac{\lambda_{\text{FSO}}}{4\pi L_{SX_n}}\right)^2}, \quad (2)$$

where σ is the geometric scattering extinction coefficient due to cloud or fog droplets, which can be evaluated as follows [21]: $\sigma_n = \left(\frac{3.91}{V_n}\right) \left(\frac{\lambda_{\text{FSO}}^{[\text{nm}]}}{550}\right)^{-q}$, where $V_n = \frac{1.002}{(KQ)^{0.6473}}$ is the visibility in kilometers, K is the liquid water content in g/m^{-3} and Q indicates the cloud concentration in m^{-3} . Furthermore, $\lambda_{\text{FSO}}^{[\text{nm}]}$ ¹ is the FSO signal's wavelength in nanometers, and q is the particle size-related coefficient defined per the Kim's model as [27]

$$q = \begin{cases} 1.6, & V_n > 50 \\ 1.3, & 6 < V_n \leq 50 \\ 0.16V_n + 0.34, & 1 < V_n \leq 6 \\ V_n - 0.5, & 0.5 < V_n \leq 1 \\ 0, & V_n \leq 0.5 \end{cases} \quad (3)$$

where the visibility bounds in the last equation are in kilometers. Also, $L_{X_n}^{(\text{eff,cloud/fog})}$ is the effective scattering length between the GS and the n th benign/malign HAP spanning only along the actual cloud or fog thickness, defined as follows [28]

$$L_{X_n}^{(\text{eff,cloud/fog, [km]})} = \frac{\Delta L^{(\text{cloud/fog, [km]})}}{\cos(\psi_{SX_n})} \quad (4)$$

where $\Delta L^{(\text{cloud/fog, [km]})}$ is the cloud/fog layer thickness and ψ_{SX_n} is the zenith angle between the GS and the n th legitimate/illegitimate HAP. On the other hand, ξ_{X_n} refers to the Mie scattering extinction coefficient caused by microscopic water particles at the sea surface, and is expressed as follows

$$\tau_{X_n} = p_1(\lambda_{\text{FSO}}) \left[h_S^{[\text{km}]}\right]^3 + p_2(\lambda_{\text{FSO}}) \left[h_S^{[\text{km}]}\right]^2 + p_3(\lambda_{\text{FSO}}) h_S^{[\text{km}]} + p_4(\lambda_{\text{FSO}}) \quad (5)$$

where $h_S^{[\text{km}]}$ is the GS altitude above the sea level in kilometers, and $p_i(\lambda)$ ($i = 1, \dots, 4$) are wavelength-dependent parameters defined as [25]

$$p_1(\lambda_{\text{FSO}}) = 0.000487 \left(\lambda_{\text{FSO}}^{[\mu\text{m}]}\right)^3 - 0.002237 \left(\lambda_{\text{FSO}}^{[\mu\text{m}]}\right)^2 + 0.003864 \lambda_{\text{FSO}}^{[\mu\text{m}]} - 0.004442, \quad (6)$$

$$p_2(\lambda_{\text{FSO}}) = -0.00573 \left(\lambda_{\text{FSO}}^{[\mu\text{m}]}\right)^3 + 0.02639 \left(\lambda_{\text{FSO}}^{[\mu\text{m}]}\right)^2 - 0.04552 \lambda_{\text{FSO}}^{[\mu\text{m}]} + 0.05164, \quad (7)$$

$$p_3(\lambda_{\text{FSO}}) = 0.02565 \left(\lambda_{\text{FSO}}^{[\mu\text{m}]}\right)^3 - 0.1191 \left(\lambda_{\text{FSO}}^{[\mu\text{m}]}\right)^2 + 0.20385 \left(\lambda_{\text{FSO}}^{[\mu\text{m}]}\right) - 0.216, \quad (8)$$

¹The notation $[x]$ in the superscript of some length parameters refers to the parameter value in x units, e.g., $\lambda_{\text{FSO}}^{[\text{nm}]}$ refers to the FSO signal wavelength in nanometers. Not specifying a unit in the superscript indicates the use of meters as a unit.

$$p_4(\lambda_{\text{FSO}}) = -0.0638 \left(\lambda_{\text{FSO}}^{[\mu\text{m}]}\right)^3 + 0.3034 \left(\lambda_{\text{FSO}}^{[\mu\text{m}]}\right)^2 - 0.5083 \lambda_{\text{FSO}}^{[\mu\text{m}]} + 0.425. \quad (9)$$

Rain attenuation contributes also to the overall path loss in vertical FSO links. In practice, rain droplets' size increases in heavy rain situations which causes additional photon refractions and scattering [21]. Carbonneau deployed an analytical model by leveraging on empirical observations of rain attenuation in FSO transmissions in [24]. The underlying rain attenuation coefficient is represented by $\delta_{SX_n}^{(\text{rain,FSO})} = 1.076\mathcal{R}^{0.67}$ (dB/km), where \mathcal{R} is the rain rate in mm/hr. It is worth highlighting that, equivalently to the cloud/fog attenuation, the rain attenuation is considered only along the rain layer thickness, as given in (2) where $L_{SX_n}^{(\text{eff,rain,[km]})}$ is the optical signal propagation length throughout the rain layer, defined as [28]

$$L_{SX_n}^{(\text{eff,rain,[km]})} = \frac{\Delta L^{(\text{rain,[km]})}}{\cos(\psi_{SX_n})}, \quad (10)$$

where $\Delta L^{(\text{rain,[km]})}$ is the rain layer thickness in km. On top of that, $G^{(\text{T,THz})}$ and $G_{X_n}^{(\text{R,THz})}$ denote the optical gains for the GS' transmit laser and the receiving HAP's photodetector, respectively, and L_{X_n} is the GS- n th legitimate/illegitimate HAP link distance. Lastly, the

As far as the turbulence-induced fading (i.e., $I_{SX_n}^{(a)}$) is concerned, Gamma-Gamma distribution has been widely adopted as a unifying distribution manifesting a wide range of turbulence regimes (i.e., from weak to strong turbulence). On the other hand, the Rayleigh pointing error model has shown a notable accuracy in representing the statistics of the fluctuation due to pointing error provoked by beam misalignment (i.e., $I_{SX_n}^{(p)}$). The next section details the mathematical representation of the received irradiance and SNR's statistics.

The receiver performs either direct detection to decode the information symbol relying on the light intensity or the coherent heterodyne one whereby either the optical signal's intensity (i.e., amplitude), phase, or frequency modulates the information symbol. To this end, the received signal-to-noise ratio (SNR) at the n th legitimate/illegitimate HAP is given as

$$\gamma_{1,X_n}^{(\text{FSO})} = \frac{(\eta\rho_{X_n} I_{SX_n})^r P_F}{\sigma_{X_n,F}^2}, \quad (11)$$

where P_F is the average transmit electrical power of the GS over the FSO link.

A. THz Link

When the ground-to-HAP transmission operates with the THz band, the propagation is affected essentially by molecular absorption, atmospheric attenuation due to cloud/fog and rain, free-space path loss, and pointing errors. As a result, the received SNR at the n th legitimate/illegitimate HAP can be expressed as

$$\gamma_{1,X_n}^{(\text{THz})} = \frac{P_T \mathcal{L}_{SX_n} \delta_{SX_n}^{(\text{rain,THz})} \delta_{SX_n}^{(\text{cloud/fog,THz})}}{\exp(\kappa_a(f) L_{SX_n}) |h_{SX_n}|^2 \sigma_{X_n,T}^2}, \quad (12)$$

where P_T is the average transmit THz signal power,

$$\mathcal{L}_{SX_n} = G^{(T, \text{THz})} G_{X_n}^{(R, \text{THz})} \left(\frac{\lambda_{\text{THz}}}{4\pi L_{SX_n}} \right)^2, \quad (13)$$

is the free-space path loss term,

$$\delta_{SX_n}^{(\text{rain, THz})} \triangleq 10^{-\frac{\vartheta(\lambda_{\text{THz}}) \mathcal{R} \nu(\lambda_{\text{THz}}) L_{X_n}^{(\text{eff, rain, [km]})}}{10}} \quad (14)$$

is the rain attenuation, where \mathcal{R} is the attenuation rate, $\vartheta(\lambda_{\text{THz}})$ and $\nu(\lambda_{\text{THz}})$ are medium- and wavelength-dependent constants for the rain attenuation,

$$\delta_{SX_n}^{(\text{cloud})} \triangleq 10^{-KM(\lambda_{\text{THz}}) L_{X_n}^{(\text{eff, cloud/fog, [km]})}} \quad (15)$$

is the cloud/fog attenuation coefficient, where $M(\lambda_{\text{THz}})$ is medium- and wavelength-dependent cloud attenuation coefficient. The values for the parameters $\vartheta(\cdot)$ and $\nu(\cdot)$ can be computed from [29, Eqs. (4), (5), Table 5] for the considered THz frequency, while the cloud/fog attenuation parameter $M(\lambda_{\text{THz}})$ can be computed using [30, Eqs. (2)-(11)]. In addition, $\kappa_a(f)$ is the frequency-dependent absorption coefficient in km^{-1} , and h_{SX_n} is the pointing errors random fluctuations term.

B. Second Hop: mmWave Link

After decoding the received signal and regenerating it, the selected legitimate HAP forwards it to the legitimate ground user U , under the presence of a malicious eavesdropping node attempting to overhear the legitimate RF signal beam. The propagation over the RF Ka-Band is less affected by molecular absorption, and beams are usually of large footprints, allowing eavesdroppers to intercept the legitimate message with higher probability. Therefore, RF transmission is not impacted by pointing errors. Nonetheless, it is worth highlighting that multipath fading and shadowing affect RF vertical links. To this end, the SNR at the legitimate/illegitimate ground receiver, given the signal is received from the n th HAP, is formulated as

$$\gamma_{2,Z}^{(\text{Ka})} = \frac{P_H \delta_{H_n Z}^{(\text{rain, Ka})} \delta_{H_n Z}^{(\text{cloud/fog, Ka})} \mathcal{L}_{H_n Z} |h_{H_n Z}|^2}{\sigma_Z^2}, Z \in \{U, E^{(2)}\}, \quad (16)$$

where P_H is the HAP transmit power, $\delta_{H_n Z}^{(\text{rain, Ka})}$ and $\delta_{H_n Z}^{(\text{cloud/fog, Ka})}$ are, Similar to the THz link, the respective rain and cloud/fog attenuation of the RF link. Also,

$$\mathcal{L}_{H_n Z} = G_{H_n}^{(T, \text{Ka})} G_Z^{(R, \text{Ka})} \left(\frac{\lambda_{\text{Ka}}}{4\pi L_{H_n Z}} \right)^2 \quad (17)$$

is the path-loss of the HAP-user link, $h_{H_n Z}$ is the complex-valued shadowed fading coefficient, modeled by the shadowed Rician distribution, and σ_Z^2 is the additive white Gaussian noise at the receiver.

III. USEFUL STATISTICS

In this section, statistical properties of the received SNR of each particular link is detailed, which will be used in the next section for the system's secrecy evaluation.

A. FSO Link

The PDF and cumulative distribution function (CDF) of the SNR $\gamma_{1, X_n}^{(\text{FSO})}$ in (11) can be expressed as [3, Eqs. (14)-(15)]

$$f_{\gamma_{1, X_n}^{(\text{FSO})}}(z) = \frac{\xi_{X_n, \text{FSO}}^2}{rz \Gamma(\alpha_{X_n}) \Gamma(\beta_{X_n})} \times G_{1,3}^{3,0} \left(\left(\frac{\mathcal{F}_{X_n, 1z}}{\gamma_{X_n}^{(\text{FSO})}} \right)^{\frac{1}{r}} \middle| \begin{matrix} -; \xi_{X_n, \text{FSO}}^2 + 1 \\ \xi_{X_n, \text{FSO}}^2, \alpha_{X_n}, \beta_{X_n}; - \end{matrix} \right), \quad (18)$$

and

$$F_{\gamma_{1, X_n}^{(\text{FSO})}}(z) = \frac{r^{\alpha_{X_n} + \beta_{X_n} - 2} \xi_{X_n, \text{FSO}}^2}{(2\pi)^{r-1} \Gamma(\alpha_{X_n}) \Gamma(\beta_{X_n})} \times G_{r+1, 3r+1}^{3r, 1} \left(\frac{\mathcal{F}_{X_n, rz}}{\gamma_{X_n}^{(\text{FSO})}} \middle| \begin{matrix} 1; \varepsilon_1^{(X_n)} \\ \varepsilon_2^{(X_n)}; 0 \end{matrix} \right), \quad (19)$$

respectively, for $X \in \{H, E^{(1)}\}$, where

$$\xi_{X_n, \text{FSO}} \triangleq \frac{w_{zeq}^{(\text{FSO})}}{2\sigma_s}, \quad (20)$$

accounts for the severity of the pointing errors, where

$$w_{zeq}^{(\text{FSO})} = w_z^{(\text{FSO})} \sqrt{\frac{\sqrt{\frac{\pi}{A_0^{(\text{FSO})}}}}{2\nu \exp(-\nu^2_{\text{FSO}})}} \quad (21)$$

refers to equivalent beam radius at the receiver plane [31] where $w_z^{(\text{FSO})}$ is the FSO beam waist at the receiver's plane,

$$A_0^{(\text{FSO})} \triangleq \text{erf}^2(\nu_{\text{FSO}}) \quad (22)$$

is the fraction of collected power in pointing error-free transmission,

$$\nu_{\text{FSO}} \triangleq \sqrt{\pi/2} R_{\text{FSO}} / w_z^{(\text{FSO})}, \quad (23)$$

R_{FSO} is the HAP's photodetector radius, and σ_s is the receiver's jitter standard deviation along the x and y axes. Additionally, α_{X_n} and β_{X_n} are the turbulence-induced fading parameters, defined for the case of untracked uplink beam as [32, Eq.]

$$\alpha_{X_n} = \left[5.95 \left(\frac{2w_0^{(\text{FSO})}}{r_0} \right)^{\frac{5}{3}} \left(\frac{\sigma_{pe}}{w_{zeq}^{(\text{FSO})}} \right)^2 + \exp \left(\frac{0.49 \sigma_{R, X_n}^2}{(1 + 0.56 \sigma_{R, X_n}^{12/5})^{7/6}} \right) - 1 \right]^{-1} \quad (24)$$

and

$$\beta_{X_n} = \left[\exp \left(\frac{0.51 \sigma_{R, X_n}^2}{(1 + 0.69 \sigma_{R, X_n}^{12/5})^{5/6}} \right) - 1 \right]^{-1},$$

respectively, where w_0 is the beam waist at the transmit GS,

$$r_0 = \left[0.42 k^2 \sec(\psi_{X_n}) \int_{h_G}^{h_{X_n}} C_n^2(h) dh \right]^{-3/5} \quad (25)$$

is the atmospheric coherence diameter with $k = 2\pi/\lambda_{\text{FSO}}$ being the wave number, and

$$C_n^2(h) = 0.00594 (\mathcal{V}/27)^2 (10^{-5}h)^{10} \exp\left(-\frac{h}{1000}\right) + 2.7 \times 10^{-16} \exp\left(-\frac{h}{1500}\right) + C_0 \exp(-h/100), \quad (26)$$

is the refractive index structure parameter in $\text{m}^{-2/3}$, where \mathcal{V} is root mean square value of the wind speed, and C_0 is the refractive index structure parameter value at the GS' altitude above sea level. Additionally,

$$\sigma_{pe} = 0.54 \left(\frac{L_S X_n \lambda_{\text{FSO}}}{2w_0^{(\text{FSO})}} \right)^2 \frac{1 - \left(\frac{\left(\frac{2\pi w_0^{(\text{FSO})}}{r_0} \right)^2}{\left(\frac{2\pi w_0^{(\text{FSO})}}{r_0} \right)^2 + 1} \right)^{1/6}}{\left(\frac{2w_0^{(\text{FSO})}}{r_0} \right)^{5/3}}. \quad (27)$$

Also,

$$\sigma_{R, X_n}^2 = 2.25 k^{\frac{7}{6}} \sec^{\frac{11}{6}}(\psi_{SX_n}) \int_{h_S}^{h_{X_n}} \left(1 - \frac{h - h_S}{h_{X_n} - h_S}\right)^{\frac{5}{6}} \times C_n^2(h) (h - h_S)^{\frac{5}{6}} dh, \quad (28)$$

is the Rytov variance of the propagation system, representing the turbulence severity level, with h_S and h_{X_n} representing the altitudes of the GS and X_n above the sea level, respectively. Furthermore, $G_{p,q}^{m,n}(\cdot)$ is the Meijer's G -function [33,

Eq. (07.34.02.0001.01)], $\mathcal{F}_{X_n, r} \triangleq \left(\frac{\xi_{X_n, \text{FSO}}^2 \alpha_{X_n} \beta_{X_n}}{r^2 (\xi_{X_n, \text{FSO}}^2 + 1)} \right)^r$, $\varepsilon_1^{(X_n)} \triangleq \left(\frac{\xi_{X_n, \text{FSO}}^2 + 1}{r} \right)_{i=1, \dots, r}$, $\varepsilon_2^{(X_n)} \triangleq \left(\frac{\xi_{X_n, \text{FSO}}^2 + i}{r}, \frac{\alpha_{X_n} + i}{r}, \frac{\beta_{X_n} + i}{r} \right)_{i=0, \dots, r-1}$,

and

$$\bar{\gamma}_{X_n}^{(\text{FSO})} = \frac{P_F \left(\eta \rho_{X_n} I_{SX_n}^{(l)} \right)^r \mathbb{E}^r \left[I_{SX_n}^{(ap)} \right]}{\sigma_{X_n, F}^2} \quad (29)$$

is the corresponding average electrical SNR with [34]

$$\mathbb{E} \left[I_{SX_n}^{(ap)} \right] = \frac{\xi_{X_n, \text{FSO}}^2 A_0^{(\text{FSO})}}{\xi_{X_n, \text{FSO}}^2 + 1}. \quad (30)$$

B. THz Link

Similarly to the FSO link, the THz channel is impacted by Rayleigh-distributed pointing errors, whereby the corresponding attenuation's magnitude, i.e., $|h_{SX_n}|$, has the following PDF

$$f_{|h_{SX_n}|}(x) = \frac{\xi_{X_n, \text{THz}}^2}{\left(A_0^{(\text{THz})} \right)^{\xi_{X_n, \text{THz}}^2}} x^{\xi_{X_n, \text{THz}}^2 - 1}, 0 < x < A_0^{(\text{THz})}, \quad (31)$$

where $\xi_{X_n, \text{THz}}^2$ is the pointing errors severity for the THz link, which can be computed equivalently to the FSO channel using (20)-(23), by substituting the FSO beam waist by the THz beam's one, and the photodetector's size by the THz antenna's physical aperture. As a consequence, armed by the Jacobian transform as well as some algebraic manipulations, one can

retrieve the PDF and CDF of the THz link's SNR, expressed in (12), as

$$f_{\gamma_{1, X_n}^{(\text{THz})}}(x) = \begin{cases} \frac{\xi_{X_n, \text{THz}}^2 \left(\frac{x}{\bar{\gamma}_{1, X_n}^{(\text{THz})}} \right)^{\xi_{X_n, \text{THz}}^2 - 1}}{2 \left(A_0^{(\text{THz})} \right)^{\xi_{X_n, \text{THz}}^2} \bar{\gamma}_{1, X_n}^{(\text{THz})}}, & \text{if } 0 < x \leq \gamma_{1, X_n}^{(\text{THz}, \max)} \\ 0, & \text{elsewhere} \end{cases}, \quad (32)$$

and

$$F_{\gamma_{1, X_n}^{(\text{THz})}}(x) = \begin{cases} \left(\frac{x}{\bar{\gamma}_{1, X_n}^{(\text{THz})}} \right)^{\xi_{X_n, \text{THz}}^2} / \left(A_0^{(\text{THz})} \right)^{\xi_{X_n, \text{THz}}^2}, & \text{if } 0 < x \leq \gamma_{1, X_n}^{(\text{THz}, \max)} \\ 1, & \text{elsewhere} \end{cases}, \quad (33)$$

respectively, where $\gamma_{1, X_n}^{(\text{THz}, \max)} \triangleq \bar{\gamma}_{1, X_n}^{(\text{THz})} \left(A_0^{(\text{THz})} \right)^2$ and

$$\bar{\gamma}_{1, X_n}^{(\text{THz})} \triangleq \frac{P_T \mathcal{L}_{SX_n} \delta_{SX_n}^{(\text{rain, THz})} \delta_{SX_n}^{(\text{cloud/fog, THz})} \mathbb{E} \left[|h_{SX_n}|^2 \right]}{\exp(\kappa_a(f) L_{SX_n}) \sigma_{X_n, T}^2} \quad (34)$$

is the average THz link's SNR with

$$\mathbb{E} \left[|h_{SX_n}|^2 \right] = \frac{\xi_{X_n, \text{THz}}^2 \left(A_0^{(\text{THz})} \right)^2}{\xi_{X_n, \text{THz}}^2 + 2}. \quad (35)$$

Remark 1. It can be noted from equations (29), (30), (34), and (35) that the average fading power due to the pointing errors for both the FSO and THz links depends on the value $\xi_{X_n, x}$ ($x \in \{\text{THz}, \text{FSO}\}$), defined in (20). This latter is proportional to the equivalent beam waist radius $w_{zeq}^{(x)}$, which is per se proportional to the beam waist (spot size) at the receiver, as shown in (21). Therefore, the higher the higher the received beam's spot size at the receiver (higher $\xi_{X_n, x}$), the greater is the corresponding moments in (30), (35) and average SNR levels in (29), (34). Consequently, this results in an increased average received SNR value.

C. MmWave Link

The HAP-to-ground user communication is performed using Ka-band RF signals that are subject to shadowed fading impairments. Abdi et al. developed in [35] a theoretical model to represent the distribution of signal attenuation in a land mobile-satellite link, for which the underlying PDF and CDF of the SNR in (16) is given as [3, Eqs. (18)-(19)]

$$f_{\gamma_{2, Z}}(x) = \frac{\phi_Z}{\bar{\gamma}_{2, Z}} \exp\left(-\frac{v_Z x}{\bar{\gamma}_{2, Z}}\right) \sum_{n=0}^{m_s^{(Z)} - 1} \frac{\left(m_s^{(Z)} - 1\right) \left(\frac{\mu_Z x}{\bar{\gamma}_{2, Z}}\right)^n}{n!} \quad (36)$$

and

$$F_{\gamma_{2, Z}}(z) = \phi_Z \sum_{n=0}^{m_s^{(Z)} - 1} \binom{m_s^{(Z)} - 1}{n} \frac{\mu_Z^n \gamma_{\text{inc}}\left(n + 1, \frac{\mu_Z z}{\bar{\gamma}_{2, Z}}\right)}{v_Z^{n+1} n!}, \quad (37)$$

respectively, where $Z \in \{U, E^{(2)}\}$, $\phi_Z \triangleq \frac{1}{2b} \left(\frac{2bm_s^{(Z)}}{2bzm_s^{(Z)} + \Omega_s^{(Z)}} \right)^{m_s}$,

$$\bar{\gamma}_{2, Z} = \frac{P_H \delta_{H_n Z}^{(\text{rain, Ka})} \delta_{H_n Z}^{(\text{cloud/fog, Ka})} \mathcal{L}_{H_n Z} \mathbb{E} \left[|h_{H_n Z}|^2 \right]}{\sigma_Z^2}, \quad (38)$$

is the average received SNR at the legitimate/illegitimate receiver, $v_Z \triangleq \zeta_Z - \mu_Z$, $\zeta_Z \triangleq \frac{1}{2b_Z}$, $2b_Z$ is the average power of multipath components, and $\mu_Z \triangleq \frac{\Omega_s^{(Z)}}{2b_Z(2b_Z m_s^{(Z)} + \Omega_s^{(Z)})}$. Additionally, $\Omega_s^{(Z)}$ is the average power of the LOS components, $m_s^{(Z)}$ is the fading severity parameter, and $\gamma_{\text{inc}}(\cdot, \cdot)$ is the lower-incomplete Gamma function [36, Eq. (9.210)].

IV. PROPOSED SCHEME AND SECRECY ANALYSIS

In this section, the proposed HAP selection scheme and the respective secrecy evaluation is detailed. In the considered network, the ground station (GS) aims at selecting one relaying HAP among the N available ones, along with the suitable transmission link (i.e., either the FSO or THz) that exhibits the highest SC. It is assumed that prior to each transmission instant, the GS has knowledge of the instantaneous channel state information of the S - H_n , S - $E_n^{(1)}$, H_n - U , and H_n - $E^{(2)}$ links, which can be used to compute the respective links' SNR levels.

A. Communication Secrecy: Background

From PLS' perspective, a confidential transmission exists if and only if the legitimate channel's capacity exceeds the malicious one's. Such a capacity difference defines the well-known SC metric as

$$C_s = [C_L - C_E]^+, \quad (39)$$

where the indices L and E refer to any pair of legitimate and illegitimate transceivers/entities in a wireless network, where

$$C_{L/E} = \log_2(1 + \gamma_{L/E}) \quad (40)$$

and $\gamma_{L/E}$ denote the malign/benign link's bandwidth-normalized channel capacity and $\gamma_{L/E}$, respectively, and $[x]^+ = \max(0, x)$. The SC defines the maximal transmission rate that can guarantee both communication reliability, i.e., successful message decoding at the legitimate receiver, and a unit equivocation rate at the eavesdropper [37]. It can be noted from (39) that the greater the legitimate link's capacity (i.e., SNR) and/or the lower the malign ones, the better the SC, thus allowing for higher secure transmission rates.

The SC is randomly fluctuating according to the wireless channel (i.e., SNR) statistics. Thus, in practice, a communication rate is fixed such that the SC unlikely falls below it. If the latter scenario occurs, a secrecy outage event takes place, where the preset communication rate R_s cannot fail in ensuring either data reliability at the legitimate receiver or the target equivocation at the eavesdropper. Therefore, the SOP is defined as [38]

$$\begin{aligned} P_s &\triangleq \Pr[C_s < R_s] \\ &= \Pr[\gamma_L < 2^{R_s} (1 + \gamma_E) - 1]. \end{aligned} \quad (41)$$

Such a probability can be expressed in terms of the PDF and CDF of the illegitimate channel's SNR and the legitimate's one, respectively, as

$$P_s = \int_{\mathcal{D}_{\gamma_E}} F_{\gamma_L} \left(2^{R_s} (1 + z) - 1 \right) f_{\gamma_E}(z) dz. \quad (42)$$

The interval \mathcal{D}_{γ_E} defines the range of the eavesdropper's SNR γ_E . Typically, $\mathcal{D}_{\gamma_E} = \mathbb{R}^+$ for most of propagation scenarios. Nonetheless, it should be pointed out that the SNR can exhibit some limit values, such as THz communication subject to pointing errors, whereby the SNR exhibits the limit $\frac{\gamma_{1, X_n}^{(\text{THz})}}{\gamma_0^{(\text{THz})}} \left(A_0^{(\text{THz})} \right)^2$.

B. Proposed Scheme

The proposed scheme's objective is to select a single HAP out of the N available ones, along with the transmission link (i.e., either THz or FSO), exhibiting the best SC. Without loss of generality, it is assumed that a perfect CSI knowledge of all the channels is available at GS for HAP/link selection. The proposed scheme's process can be detailed as follows:

- 1) The GS inspects the CSI of the channels with respect to the N legitimate and illegitimate HAPs over both the THz and FSO links, which can be obtained by feedback links. At the same time, each HAP estimates its CSI from the legitimate and illegitimate ground receivers through the same mechanism.
- 2) Then, the measured second-hop CSI values are sent back to the GS to compute the corresponding legitimate and illegitimate SNRs, and, consequently, the secrecy capacity of each link using (39) and (40).
- 3) Then, for each of the N haps, the GS selects the link $\ell \in \{\text{THz}, \text{FSO}\}$ according to the following rule

$$\ell = \begin{cases} \text{FSO, if } C_{s,1,\text{FSO}}^{(n)} \geq R_s \\ \text{THz, if } C_{s,1,\text{FSO}}^{(n)} < R_s, C_{s,1,\text{THz}}^{(n)} \geq R_s \end{cases} \quad (43)$$

where $C_{s,1,\text{FSO}}^{(n)}$ and $C_{s,1,\text{THz}}^{(n)}$ are the respective FSO and THz channels' SCs, which can be expressed using (39), (40), and the SNR expression in (11) and (12). It is worth mentioning that the third case when both SCs fall below R_s is identified as a communication outage, where transmission is suspended.

- 4) The GS selects the best HAP H_{n^*} encompassing the highest end-to-end (e2e) SC as

$$n^* = \arg \max_{n=1, \dots, N} C_s^{(n)}, \quad (44)$$

where

$$C_s^{(n)} = \min \left(C_{s,1,\ell}^{(n)}, C_{s,2,\text{Ka}}^{(n)} \right) \quad (45)$$

is the e2e SC of the dual-hop link via the n th HAP operating with decode-and-forward (DF) relaying and $C_{s,2,\text{Ka}}^{(n)}$ is the corresponding second hop's SC over the RF link.

C. Secrecy Evaluation of the Proposed Scheme

Proposition 1. *The SOP of the proposed scheme can be formulated as*

$$P_s = \prod_{n=1}^N \left[P_{s,\text{FSO}}^{(1,n)} P_{s,\text{THz}}^{(1,n)} + P_{s,\text{Ka}}^{(2,n)} - P_{s,\text{FSO}}^{(1,n)} P_{s,\text{THz}}^{(1,n)} P_{s,\text{Ka}}^{(2,n)} \right]. \quad (46)$$

where $P_{s,\text{FSO}}^{(1,n)}$, $P_{s,\text{THz}}^{(1,n)}$, and $P_{s,\text{Ka}}^{(2,n)}$ indicate the SOP of the FSO, THz, and Ka-band RF links

$$P_{s,FSO}^{(1,n)} = \frac{r^{\alpha_{E_n} + \beta_{E_n} + \alpha_{H_n} + \beta_{H_n} - 3} \xi_{E_n,FSO}^2 \xi_{H_n,FSO}^2}{r (2\pi)^{2(r-1)} \Gamma(\alpha_{H_n}) \Gamma(\beta_{H_n}) \Gamma(\alpha_{E_n}) \Gamma(\beta_{E_n})} \times \left[\begin{array}{l} G_{0,1;r+2,3r+1;r+1,3r}^{1,0;3r,1} \left(Q_{H_n}, Q_{E_n} \left| \begin{array}{l} -; - : 1; \varepsilon_1^{(H_n)}, 0 : 1; \varepsilon_1^{(E_n)} \\ 1; - : \varepsilon_2^{(H_n)}; 0 : \varepsilon_2^{(E_n)}; - \end{array} \right. \right) \\ - \frac{\prod_{i=0}^{r-1} \Gamma\left(\frac{\xi_{E_n,FSO}^2 + i}{r}\right) \Gamma\left(\frac{\alpha_{E_n} + i}{r}\right) \Gamma\left(\frac{\beta_{E_n} + i}{r}\right)}{\prod_{i=1}^r \Gamma\left(\frac{\xi_{E_n,FSO}^2 + i}{r}\right)} G_{3r+1;3r+1}^{3r,1} \left(Q_{H_n}, Q_{E_n} \left| \begin{array}{l} 1; \varepsilon_1^{(H_n)} \\ \varepsilon_2^{(H_n)}; 0 \end{array} \right. \right) \end{array} \right] \quad (47)$$

$$P_{s,THz}^{(1,n)} = \begin{cases} \frac{\xi_{E_n,THz}^2 (\bar{\gamma}_{1,H_n}^{(THz)})^{-\frac{\xi_{H_n,THz}^2}{2}}}{2(A_0^{(THz)})^{\xi_{H_n,THz}^2 + \xi_{E_n,THz}^2} (\bar{\gamma}_{1,E_n}^{(THz)})^{\frac{\xi_{E_n,THz}^2}{2}}} \\ \times {}_2F_1 \left(-\frac{\xi_{E_n,THz}^2}{2}, \frac{\xi_{E_n,THz}^2}{2}; \frac{\xi_{E_n,THz}^2}{2} + 1; -\frac{2^{R_s} \min(\Psi_{1,H_n}, \gamma_{1,E_n}^{(THz,max)})}{2^{R_s} - 1} \right) \\ + F_{\gamma_{SE_n}^{(THz)}} \left(\gamma_{1,E_n}^{(THz,max)} \right) - F_{\gamma_{SE_n}^{(THz)}} \left(\Psi_{1,H_n} \right), \text{ if } \Psi_{1,H_n} > 0 \\ 1, \text{ if } \Psi_{1,H_n} < 0 \end{cases} \quad (48)$$

$$P_{s,Ka}^{(2,n)} = \frac{\phi_U \phi_{E^{(2)}} \exp\left(-\frac{v_{E^{(2)}} \left[\frac{1}{2^{R_s}} - 1\right]}{\bar{\gamma}_{2,E^{(2)}}}\right)}{2^{R_s} \bar{\gamma}_{2,E^{(2)}}} \sum_{n=0}^{m_s^{(E^{(2)})} - 1} \sum_{p=0}^{m_s^{(U)} - 1} \frac{(m_s^{(E^{(2)})} - 1)!}{n!} \left(\frac{\mu_{E^{(2)}}}{2^{R_s} \bar{\gamma}_{2,E^{(2)}}}\right)^n \frac{(m_s^{(U)} - 1)!}{p!} \mu_U^p \\ \times \sum_{q=0}^n \frac{\binom{n}{q}}{(1 - 2^{R_s})^{q-n}} \left[\begin{array}{l} \left(\frac{\bar{\gamma}_{2,E^{(2)}} 2^{R_s}}{v_{E^{(2)}}}\right)^{q+1} \Gamma_{\text{inc}}\left(q+1, \frac{v_{E^{(2)}} (2^{R_s} - 1)}{\bar{\gamma}_{2,E^{(2)}} 2^{R_s}}\right) \\ - \sum_{k=0}^p \frac{\left(\frac{v_U}{\bar{\gamma}_{2,U}}\right)^k \Gamma_{\text{inc}}\left(k+q+1, (2^{R_s} - 1) \left[\frac{v_U}{\bar{\gamma}_{2,U}} + \frac{v_{E^{(2)}}}{\bar{\gamma}_{2,E^{(2)}} 2^{R_s}}\right]\right)}{\left[\frac{v_U}{\bar{\gamma}_{2,U}} + \frac{v_{E^{(2)}}}{\bar{\gamma}_{2,E^{(2)}} 2^{R_s}}\right]^{k+q+1}} \frac{1}{k!} \end{array} \right] \quad (49)$$

Proof. Kindly refer to Appendix A. \square

Remark 2. It can be seen from equation (46) that the overall system's SOP is expressed in terms of the individual per-link and per-hop SOP, independently. Therefore, the quantification of each of the underlying link's SOP can provide an overall system's SOP evaluation.

Proposition 2. The SOP of the individual FSO, THz, and RF links, given the communication is performed through the n th HAP, can be expressed in (47), (48), and (49), respectively, shown at the top of the current and next page where $G_{\dots}(\dots, \dots)$ is the bivariate Meijer's G -function [39],

$$Q_{H_n} \triangleq \left(\frac{\xi_{H_n,FSO}^2 \alpha_{H_n} \beta_{H_n}}{r^2 (\xi_{H_n,FSO}^2 + 1)} \right)^r \frac{2^R - 1}{\bar{\gamma}_{H_n}^{(FSO)}}, \quad (50)$$

$$Q_{E_n} \triangleq \left(\frac{\xi_{E_n,FSO}^2 \alpha_{E_n} \beta_{E_n}}{r^2 (\xi_{E_n,FSO}^2 + 1)} \right)^r \frac{1 - \frac{1}{2^R}}{\bar{\gamma}_{E_n}^{(FSO)}}, \quad (51)$$

${}_2F_1(\dots, \dots; \dots)$ is the Gauss hypergeometric function [33, Eq. (07.23.02.0001.01)], $\Psi_{1,H_n} \triangleq \frac{\gamma_{1,H_n}^{(THz,max)} + 1}{2^{R_s}} - 1$, and $\Gamma_{\text{inc}}(\dots, \dots)$ stands for the upper incomplete Gamma function [36, Eq. (8.350.2)].

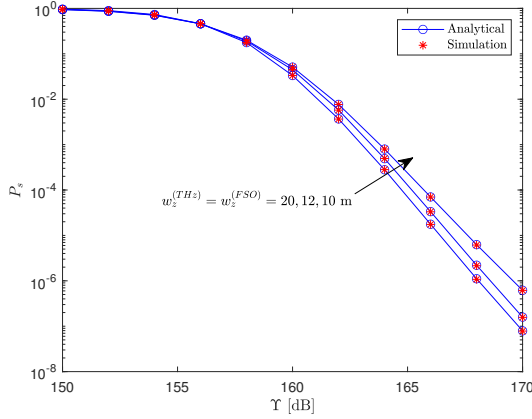
Proof. Kindly refer to Appendix B. \square

V. NUMERICAL EVALUATION

In this section, numerical results of the proposed scheme's secrecy are presented to manifest its secrecy performance with respect to the various system parameters incorporated. Unless otherwise mentioned, the considered system parameter values are highlighted in Table I. Throughout the results' figures, the analytical curves were plotted by evaluating the analytical SOP expression by (46), (47), (48), and (49). In addition, it is worth highlighting that Monte Carlo simulation results were obtained by generating 3×10^6 random values to mimic each link's random fading attenuation, per the distributions in (18), (32), and (36). Also, the numerical results were evaluated by setting $\Upsilon_{H_n} = \Upsilon_{U_n} = \Upsilon$, where $\Upsilon_{H_n} = \frac{P_{E_n}}{\sigma_{H_n,FSO}^2}$ is the transmit SNR

Parameter [unit]	Value	Parameter [unit]	Value
η	1	$G^{(T,FSO)}, G^{(R,FSO)}$ [dBi]	10^{12} [26]
ρ_{H_n}	2/3	$G^{(T,THz)}, G^{(R,THz)}$ [dBi]	10^5
r	2	λ_{THz} [mm]	1.5
λ_{FSO} [nm]	1550	$w_0^{(FSO)}$ [cm]	2
K [g/m ³]	0.064 [14]	\mathcal{V} [m/s]	21
Q [cm ⁻³]	0.025 [14]	$w_z^{(FSO)}, w_z^{(THz)}$ [m]	15
$\Delta L^{(cloud)}$ [km]	5	σ_s [m]	10
$\Delta L^{(fog)}$ [km]	0.3	$m_s^{(Z)}$	19
$\psi_{SX_n}, \psi_{H_n, Z}$ [deg]	30	$\Omega_s^{(Z)}$	1.29
$h_S^{[km]}$	0.01	b_Z	0.158
κ_a [km ⁻¹] [40]	4.4×10^{-3}	R_s [bps/Hz]	3

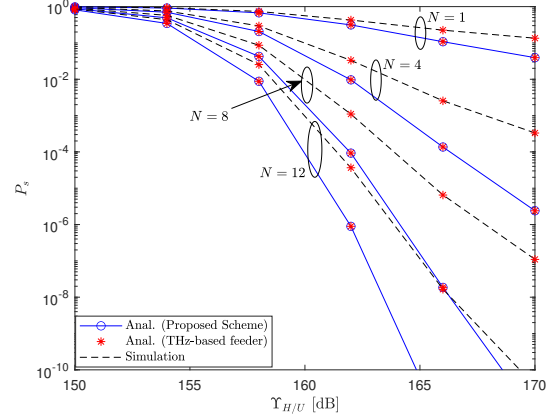
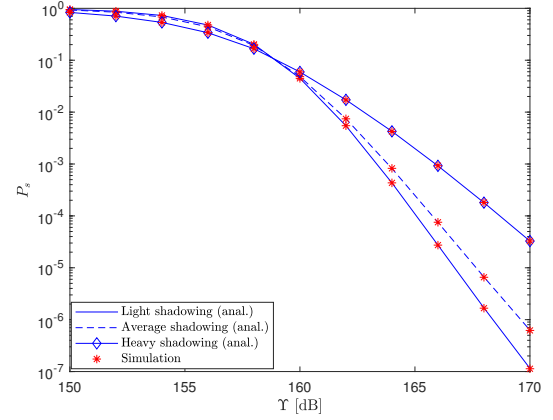
TABLE I: Simulation parameters' values.

Fig. 2: SOP of the proposed scheme vs. Υ for different beam waist values.

of the first hop over either the FSO/THz links, while $\Upsilon_U = P_H/\sigma_U^2$, whereas $\Upsilon_{E_n^{(1)}} = \Upsilon_{E_n^{(2)}} = 130$ dB.

Fig. 2 presents the system's secrecy in terms of the average legitimate transmit SNR Υ for different values of the received beam waist for the FSO and THz links, i.e., $w_z^{(FSO)}$ and $w_z^{(THz)}$. It is observed that the system's secrecy is enhanced i.e., decreasing SOP, with the increase of the beam's spot size at the receiver. This is due to the fact that the greater the beam waist at the receiver plane, the smaller the impact of the severity of the pointing errors, i.e., higher $\xi_{X_n, FSO}^2$ and $\xi_{X_n, THz}^2$, which results in a higher average received SNR, as shown in Remark 1.

In Fig. 3, the system's SOP performance is shown versus the legitimate transmit SNR Υ for different values of the number of HAPs N . One can ascertain that the increase in the number of HAPs results in a system's secrecy flourishing, where the SOP can reach 10^{-10} with $\Upsilon = 165$ dB and $N = 12$. In addition, it can also be noted that at high Υ values, the SOP improves by four orders of magnitude when increasing the number of HAPs from $N = 1$ (benchmark single-HAP system) to $N = 4$. Furthermore, to gain better insights into the system's secrecy gain, a comparison with a benchmark scheme relying solely on the THz feeder link is performed. It is obvious that the proposed hybrid FSO/THz results in better secrecy enhancement with respect to the THz-feeder-link transmission system, where the secrecy gain can reach around 4 and 5 dB at $P_s = 10^{-6}$ and $P_s = 10^{-10}$, respectively.

Fig. 3: SOP of the proposed scheme vs. Υ for different N values.Fig. 4: SOP of the proposed scheme vs. Υ for different RF shadowing scenarios.

The scheme's secrecy performance is shown in Fig. 4 with respect to different second hop's RF shadowing scenarios, namely light, average (mild), and strong shadowing scenarios. To this end, the corresponding fading parameters for the aforementioned scenarios are set, respectively, as $(m_s^{(Z)} = 19, \Omega_s^{(Z)} = 1.29, b_Z = 0.158)$, $(m_s^{(Z)} = 10, \Omega_s^{(Z)} = 0.835, b_Z = 0.126)$, and $(m_s^{(Z)} = 1, \Omega_s^{(Z)} = 8.97 \times 10^{-4}, b_Z = 0.063)$, as considered in [35]. The system's SOP shows an enhancement in the light shadowing regime where it can reach a level of 10^{-7} with $\Upsilon = 170$ dB, whereas a drop by around one and two orders of magnitude is manifested when the second hop's RF propagation is under moderate and strong shadowing cases, respectively.

Fig. 4 presents the scheme's SOP in terms of varying values of the zenith angle (ψ_{SX_n}) between the GS and the N HAPs. We consider that $\Upsilon = 150$ dB, while $\Upsilon_{E_n^{(1)}} = \Upsilon_{E_n^{(2)}} = 130$ dB. In order to get more insights on other physical parameters, such as the HAPs altitude, the performance is shown for different values of the latter parameter. Several observations can be made from this figure. For instance, it is ascertained that,

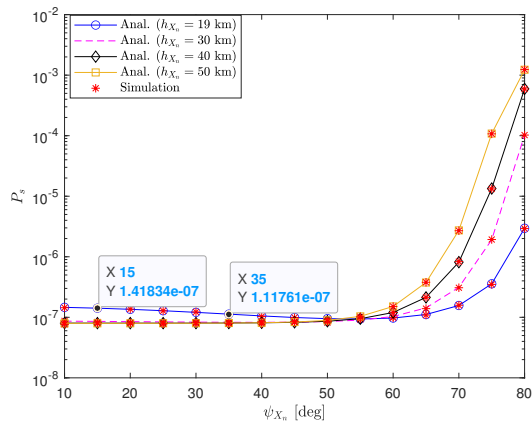
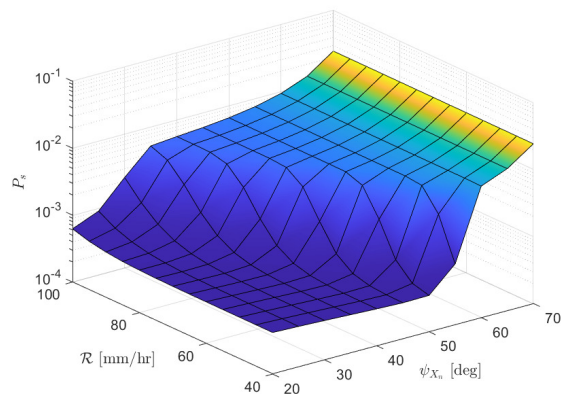


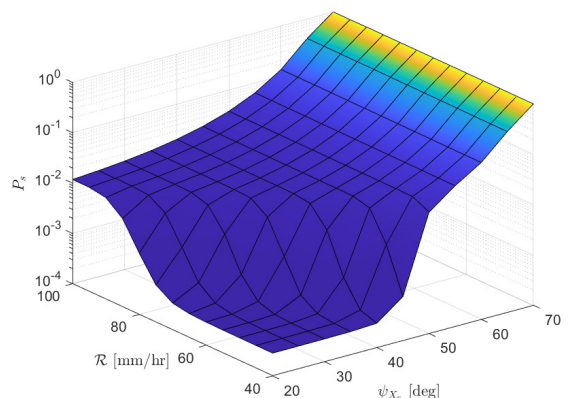
Fig. 5: SOP of the proposed scheme vs. ψ_{SX_n} for different HAPs altitude.

for a HAP altitude of 19 km, the system's secrecy flourishes in spite of the increase in ψ_{SX_n} . This is due to the fact that, for a relatively lower HAPs altitude, the FSO, THz, and RF signals are less affected by the distance-dependant free-space path loss, which results in a high average SNR levels at both legitimate and illegitimate terminals. The increase in ψ_{SX_n} between 0° and 60° results in a higher path loss attenuation as the GS-HAP distance can be expressed as $L_{SX_n} = \frac{h_{X_n} - h_S}{\cos(\psi_{SX_n})}$. Therefore, this results in an SNR degradation for the legitimate and illegitimate channels, where one can conclude that the secrecy enhancement in such a high SNR regime is mainly dominated by degrading the illegitimate channel's SNR. For $\psi_{SX_n} > 60^\circ$, the SOP increases due to increased path-loss, significantly degrading the SNRs of both types of link. For instance, a SOP of 10^{-3} can be reached with $N = 4$ HAPs at 50 km of altitude. It can be also noted that low HAPs altitude (i.e., high received average SNR) for lower zenith angle values results in a slight secrecy degradation compared to higher HAPs altitudes. This is also due to the fact that for lower zenith angles, a lower altitude yields a high average SNR at the malign and benign HAPs, where the secrecy enhancement is mainly dominated by the degradation in the illegitimate channel's SNR (increasing HAPs altitude) rather than the increase of the legitimate channel's one.

In Fig. 6, the proposed scheme's performance is shown as a function of different levels of precipitation rates and zenith angles. It is worth mentioning that the curves were obtained by setting $R_s = 5$ bps/Hz and $\rho_{H_n} = 3/4$, while the SOP performance is shown versus Y_H , with Y_U [dB] = Y_H [dB] + 30, $Y_{E(1)} = 130$ dB, and $Y_{E(2)} = 160$ dB. One can note the secrecy degradation of the considered scheme with the increase in the rain rate and zenith angle, where a SOP level of 2.4% can be reached at a precipitation rate $\mathcal{R} = 100$ mm/hr (i.e., heavy rain) with a zenith angle $\psi_{SX_n} = 70^\circ$ at $h_{X_n} = 19$ km, while a SOP of unit (i.e., worst secrecy scenario is reached at $h_{X_n} = 40$ km at the same aforementioned rain rate and zenith angle levels. Thus, the average SNRs of the FSO, THz, and RF links are attenuated, yielding a decrease in the respective link's SCs and an increase in their SOPs, degrading the total SOP. It is worth mentioning that the rain attenuation effect is more significant



(a) $h_{X_n} = 19$ km.



(b) $h_{X_n} = 40$ km.

Fig. 6: SOP of the proposed scheme vs. the rain rate (\mathcal{R}) and the zenith angle ψ_{X_n} .

in zenith angle values between 20° and 60° .

Fig. 7 depicts the analyzed scheme's secrecy performance for different levels of fog. The figure's curves were obtained by setting $R_s = 5$ bps/Hz and $\rho_{H_n} = 3/4$. Results show that the system's secrecy exhibits a significant degradation at a dense fog regime for a zenith angle $\psi_{X_n} = 50^\circ$, where the secrecy loss can reach around 4 and 5 dB with respect to the thick, light, and moderate types of fog. It is worth noting also that at a lower zenith angle value, i.e., $\psi_{X_n} = 30^\circ$, the scheme's secrecy is equal for light, moderate, and thick fog types, while it shows a secrecy loss of 3 dB with respect to the dense fog type. This is due to the fact that at lower ψ_{X_n} , the free-space path loss is less significant, and the transmit SNR can compensate for the fog loss and the free-space path loss at both the legitimate and illegitimate HAPs.

VI. CONCLUSION

In this paper, a secrecy-enhancing scheme for a HAP-aided hybrid terrestrial-aerial transmission network was proposed. In particular, the proposed scheme relied on the adoption of a THz feeder link as a backup for the FSO one, whenever the latter one fails in achieving a target SC level. In addition,

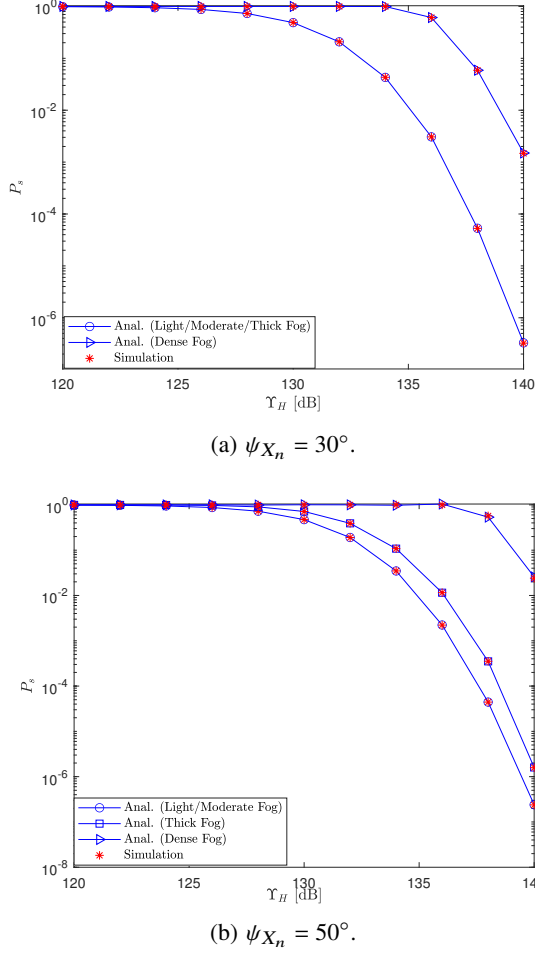


Fig. 7: SOP of the proposed scheme vs. Υ_H for different fog regimes.

the proposed scheme utilizes multi-HAP diversity to combat eavesdropping through the presence of multiple relaying HAPs. A closed-form expression for the overall system's SOP was derived encompassing the key parameters of the considered scheme. Obtained results manifested the secrecy enhancement of the proposed scheme with the increase of the FSO and THz beam spot size at the receiver when transmitting in light or moderate RF signals shadowing, or the decrease of HAPs' zenith angles with respect to the GS at higher altitudes. Furthermore, it has been shown that the proposed scheme exhibits higher secrecy compared to the benchmark single-HAP and FSO-based feeder link scheme, where both (i) HAPs diversity and (ii) the presence of the backup THz link significantly contribute to enhancing the security level of the network. Precisely, results manifested a SOP decrease by N orders of magnitude at the high SNR level when raising the number of HAPs from a unit to N . Furthermore, a 5-dB secrecy gain is manifested with respect to the benchmark FSO-based one at high SNR levels.

APPENDIX A: PROOF OF PROPOSITION 1

The proposed scheme is based on switching between the THz and FSO links per their respective SCs, where the

FSO link is primarily adopted whenever its SC exceeds a communication threshold rate R_s . Otherwise, the THz link is activated if its SC surpasses R_s . Therefore, an outage event takes place when both links' SCs are less than R_s . Thus, we can formulate the SOP of the first hop link for the pair of legitimate/illegitimate HAPs, i.e., H_n/E_n , as

$$P_s^{(1,n)} = \Pr \left[C_{s,1,FSO}^{(n)} \leq R_s, C_{s,1,THz}^{(n)} \leq R_s \right] \quad (52)$$

As both the FSO and THz links are independent, the expression in (52) can be reformulated as

$$P_s^{(1,n)} = \Pr \left[\underbrace{C_{s,1,FSO}^{(n)} \leq R_s}_{\triangleq P_{s,FSO}^{(1,n)}} \underbrace{C_{s,1,THz}^{(n)} \leq R_s}_{\triangleq P_{s,THz}^{(1,n)}} \right] \quad (53)$$

On the other hand, when DF relaying is implemented, it is established that the e2e SC of DF-based dual-hop wireless networks is the minimum of the two hops' SCs. Henceforth, an outage in at least one of the two hops results in an e2e outage event. Thus, for a given pair H_n/E_n , the e2e SOP is expressed a

$$\begin{aligned} P_s^{(n)} &= P_s^{(1,n)} \left(1 - P_{s,Ka}^{(2,n)} \right) + \left(1 - P_s^{(1,n)} \right) P_{s,Ka}^{(2,n)} + P_s^{(1,n)} P_{s,Ka}^{(2,n)} \\ &= P_s^{(1,n)} + P_{s,Ka}^{(2,n)} - P_s^{(1,n)} P_{s,Ka}^{(2,n)}, \end{aligned} \quad (54)$$

where

$$P_{s,Ka}^{(2,n)} = \Pr \left[C_{s,2,Ka}^{(n)} \leq R_s \right] \quad (55)$$

is the second hop's SC. As a result, the e2e SOP of the dual-hop link through the n th HAP is expressed from (53)-(55) as

$$P_s^{(n)} = P_{s,FSO}^{(1,n)} P_{s,THz}^{(1,n)} + P_{s,Ka}^{(2,n)} - P_{s,FSO}^{(1,n)} P_{s,THz}^{(1,n)} P_{s,Ka}^{(2,n)}, \quad (56)$$

Finally, as the proposed scheme picks the HAP exhibiting the greatest SC (i.e., lowest SOP), it can be inferred that a secrecy outage event occurs only if all the N links (through the N HAPs) are in outage, that is

$$\begin{aligned} P_s &= \prod_{n=1}^N P_s^{(n)} \\ &= \prod_{n=1}^N \left[P_{s,FSO}^{(1,n)} P_{s,THz}^{(1,n)} + P_{s,Ka}^{(2,n)} - P_{s,FSO}^{(1,n)} P_{s,THz}^{(1,n)} P_{s,Ka}^{(2,n)} \right] \end{aligned} \quad (57)$$

which concludes the proposition's proof.

APPENDIX B: PROOF OF PROPOSITION 2

A. FSO Link

The SOP of the n th FSO link (i.e., $S-H_n$) can be expressed by inserting the CDF in (19) with $X = H_n$ and the PDF in (18) with $X = E^{(1)}$ into (42) as

$$\begin{aligned} F_{\gamma_{1,X_n}}^{(FSO)}(z) &= \frac{r^{\alpha X_n + \beta X_n - 2} \xi_{X_n,FSO}^2}{(2\pi)^{r-1} \Gamma(\alpha X_n) \Gamma(\beta X_n)} \\ &\quad \times G_{r+1,3r+1}^{3r,1} \left(\left(\frac{\mathcal{G}_{X_n}}{\gamma_{X_n}^{(FSO)}} z \right)^r \middle| \begin{matrix} 1; \varepsilon_1^{(X_n)} \\ \varepsilon_2^{(X_n)}; 0 \end{matrix} \right), \end{aligned} \quad (58)$$

$$P_{s,\text{FSO}}^{(1,n)} \stackrel{(a)}{=} \frac{\xi_{E_n,\text{FSO}}^2}{r\Gamma(\alpha_{E_n})\Gamma(\beta_{E_n})} \frac{r^{\alpha_{H_n}+\beta_{H_n}-2}\xi_{H_n,\text{FSO}}^2}{(2\pi)^{r-1}\Gamma(\alpha_{H_n})\Gamma(\beta_{H_n})}$$

$$\times \int_0^\infty G_{1,3}^{3,0} \left(\mathcal{F}_{E_n,1} \left(\frac{z}{\gamma_{E_n}^{(\text{FSO})}} \right) \middle| \begin{matrix} -; \xi_{E_n,\text{FSO}}^2 + 1 \\ \xi_{E_n,\text{FSO}}^2, \alpha_{E_n}, \beta_{E_n}; - \end{matrix} \right)$$

$$\times G_{r+1,3r+1}^{3r,1} \left(\frac{\mathcal{F}_{H_n^{(1)},r,z}}{\gamma_{H_n}^{(\text{FSO})}} \middle| \begin{matrix} 1; \varepsilon_1^{(H_n)} \\ \varepsilon_2^{(H_n)}; 0 \end{matrix} \right) \quad (59a)$$

$$\stackrel{(b)}{=} \frac{\xi_{E_n,\text{FSO}}^2 \xi_{H_n,\text{FSO}}^2 (2\pi)^{1-r} r^{\alpha_{H_n}+\beta_{H_n}-3}}{\Gamma(\alpha_{E_n})\Gamma(\alpha_{H_n})\Gamma(\beta_{E_n})\Gamma(\beta_{H_n})} \frac{1}{2\pi j}$$

$$\int_{C_s} \left[\mathcal{F}_{X_n,r} \frac{2^R}{\gamma_{H_n}^{(\text{FSO})}} \right]^{-s} \mathcal{T}_{H_n}(r,s) \int_0^\infty \frac{z^{-1}}{\left(z+1-\frac{1}{2^R}\right)^s}$$

$$\times G_{1,3}^{3,0} \left(\mathcal{F}_{E_n,1} \left(\frac{z}{\gamma_{E_n}^{(\text{FSO})}} \right) \middle| \begin{matrix} -; \xi_{E_n,\text{FSO}}^2 + 1 \\ \xi_{E_n,\text{FSO}}^2, \alpha_{E_n}, \beta_{E_n}; - \end{matrix} \right) ds \quad (59b)$$

with

$$\mathcal{T}_{H_n}(r,s) = \frac{\prod_{i=0}^{r-1} \Gamma\left(\frac{\xi_{H_n,\text{FSO}}^2+i}{r} + s\right) \Gamma\left(\frac{\alpha_{H_n}+i}{r} + s\right) \Gamma\left(\frac{\beta_{H_n}+i}{r} + s\right)}{(-s) \prod_{i=1}^r \Gamma\left(\frac{\xi_{H_n,\text{FSO}}^2+i}{r}\right)} \quad (60)$$

where Step (b) in (59b) stems from Step (a) through the Mellin-Barnes representation of the Meijer's G -function in [33, Eq. (07.34.02.0001.01)]. Thus, relying on the identity [33, Eq. (07.34.21.0086.01)] and some algebraic manipulations, it yields

$$P_{s,\text{FSO}}^{(1,n)} = \frac{\xi_{E_n,\text{FSO}}^2 \xi_{H_n,\text{FSO}}^2 r^{\alpha_{E_n}+\beta_{E_n}+\alpha_{H_n}+\beta_{H_n}-3}}{r(2\pi)^{2(r-1)} \Gamma(\alpha_{E_n})\Gamma(\beta_{E_n})\Gamma(\alpha_{H_n})\Gamma(\beta_{H_n})} \left(\frac{1}{2\pi j}\right)^2$$

$$\times \int_{C_s} \int_{C_v} \mathcal{T}_{H_n}(r,s) \Gamma(1-v) \mathcal{T}_{E_n}(r,v) Q_{H_n}^{-s} Q_{E_n}^{-v} ds dv. \quad (61)$$

It is worthwhile that the double complex integral above requires the following conditions on the complex contours of integral, i.e., $C_s =]c_s - j\infty, c_s + j\infty[$, $C_v =]c_v - j\infty, c_v + j\infty[$, as

$$c_s \in \left[-\frac{\min(\xi_{H_n,\text{FSO}}^2, \alpha_{H_n}, \beta_{H_n})}{2}, 0 \right] \iff c_s < 0, \quad (62)$$

which implies that the poles of $\Gamma(-v)$ and $\Gamma(s+v)$ will overlap as $c_v > 0$ to guarantee a non-overlapping of the poles of the second integral. Thus, residues on poles of $\Gamma(-v)$ from the first pole $v = 0$ up to c_v must be subtracted from the double integral term in (61). Therefore, relying on the aforementioned subtraction and the bivariate Meijer's G -function representation in [39], it yields (47).

B. THz Link

By incorporating the CDF in (33) with $X = H_n$ and the PDF in (32) with $X = E_n$ into (42), the SOP of the first hop's

n th link (S - H_n) link when operating with the THz band can be expressed as

$$P_{s,\text{THz}}^{(1,n)} = \int_0^{\gamma_{1,E_n}^{(\text{THz,max})}} F_{\gamma_{SH_n}^{(\text{THz})}} \left(2^{R_s} (z+1) - 1 \right) f_{\gamma_{SE_n}^{(\text{THz})}}(z) dz. \quad (63)$$

where $\gamma_{1,E_n}^{(\text{THz,max})}$ and Ψ_{1,H_n} are defined in the proposition. It can be observed that the integral in the last equation can exhibit three cases, per the intervals defining the legitimate link's CDF as:

1) *Case 1:* $\gamma_{1,E_n}^{(\text{THz,max})} > \Psi_{1,H_n} > 0$: In such a scenario, the integral in (63) can be expressed as the sum of two terms, as the legitimate link's CDF term in (63) equals unit for $z > \Psi_{1,H_n}$, as can be deduced from (33). Thus, it yields

$$P_{s,\text{THz}}^{(1,n)} \stackrel{(a)}{=} \frac{(2^{R_s} - 1)^{\frac{\xi_{H_n,\text{THz}}^2}{2}} \xi_{E_n,\text{THz}}^2 \left(\gamma_{1,H_n}^{(\text{THz})}\right)^{-\frac{\xi_{H_n,\text{THz}}^2}{2}}}{2 \left(A_0^{(\text{THz})}\right)^{\xi_{H_n,\text{THz}}^2 + \xi_{E_n,\text{THz}}^2} \left(\gamma_{1,E_n}^{(\text{THz})}\right)^{\frac{\xi_{E_n,n,\text{THz}}^2}{2}}}$$

$$\times \int_0^{\Psi_{1,H_n}} \frac{z^{\frac{\xi_{E_n,\text{THz}}^2}{2} - 1}}{\left(\frac{2^{R_s}}{2^{R_s}-1}z + 1\right)^{-\frac{\xi_{H_n,\text{THz}}^2}{2}}} dz$$

$$+ \frac{\xi_{E_n,n,\text{THz}}^2}{2 \left(A_0^{(\text{THz})}\right)^{\xi_{E_n,\text{THz}}^2} \gamma_{1,E_n}^{(\text{THz})}} \int_{\Psi_{1,H_n}}^{\gamma_{1,E_n}^{(\text{THz,max})}} \left(\frac{z}{\gamma_{1,E_n}^{(\text{THz})}}\right)^{\frac{\xi_{E_n,n,\text{THz}}^2}{2} - 1} dz \quad (64a)$$

$$\stackrel{(b)}{=} \frac{(2^{R_s} - 1)^{\frac{\xi_{H_n,\text{THz}}^2}{2}} \xi_{E_n,n,\text{THz}}^2 \left(\gamma_{1,H_n}^{(\text{THz})}\right)^{-\frac{\xi_{H_n,\text{THz}}^2}{2}}}{2 \left(A_0^{(\text{THz})}\right)^{\xi_{H_n,\text{THz}}^2 + \xi_{E_n,n,\text{THz}}^2} \left(\gamma_{1,E_n}^{(\text{THz})}\right)^{\frac{\xi_{E_n,n,\text{THz}}^2}{2}}}$$

$$\times {}_2F_1 \left(-\frac{\xi_{H_n,\text{THz}}^2}{2}, \frac{\xi_{E_n,\text{THz}}^2}{2}; \frac{\xi_{E_n,\text{THz}}^2}{2} + 1; -\frac{2^{R_s} \Psi_{1,H_n}}{2^{R_s} - 1} \right)$$

$$+ F_{\gamma_{SE_n}^{(\text{THz})}} \left(\gamma_{1,E_n}^{(\text{THz,max})} \right) - F_{\gamma_{SE_n}^{(\text{THz})}} \left(\Psi_{1,H_n} \right) \quad (64b)$$

where Step (b) is reached by utilizing [36, Eq. (3.194.1)] for computing the first term, while the second term of Step (a) yields the difference of CDF values at the two specified integration bounds, i.e., Ψ_{1,H_n} and $\gamma_{1,E_n}^{(\text{THz,max})}$.

2) *Case 2:* $\gamma_{1,E_n}^{(\text{THz,max})} < \Psi_{1,H_n}$: In this case, the integral of (63) is truncated to $\gamma_{1,E_n}^{(\text{THz,max})}$ as the PDF vanishes for values exceeding the aforementioned bound. Therefore, this yields, similarly to Case 1, the

$$P_{s,\text{THz}}^{(1,n)} = \frac{(2^{R_s} - 1)^{\frac{\xi_{H_n,\text{THz}}^2}{2}} \xi_{E_n,n,\text{THz}}^2 \left(\gamma_{1,H_n}^{(\text{THz})}\right)^{-\frac{\xi_{H_n,\text{THz}}^2}{2}}}{2 \left(A_0^{(\text{THz})}\right)^{\xi_{H_n,\text{THz}}^2 + \xi_{E_n,n,\text{THz}}^2} \left(\gamma_{1,E_n}^{(\text{THz})}\right)^{\frac{\xi_{E_n,n,\text{THz}}^2}{2}}}$$

$$\times {}_2F_1 \left(-\frac{\xi_{H_n,\text{THz}}^2}{2}, \frac{\xi_{E_n,\text{THz}}^2}{2}; \frac{\xi_{E_n,\text{THz}}^2}{2} + 1; -\frac{2^{R_s} \gamma_{1,E_n}^{(\text{THz,max})}}{2^{R_s} - 1} \right) \quad (65)$$

3) *Case 3: $\Psi_{1,H_n} < 0$* : This third case is manifested when the CDF's argument in (63) is always above the integral's upper bound for all integration values, i.e., $2^{R_s}(z+1) - 1 > \gamma_{1,E_n}^{(\text{THz,max})} \forall z > 0$. Thus, $F_{\gamma_{SE_n}^{(\text{THz})}}(2^{R_s}(z+1) - 1) = 1$ for $z \in [0, \gamma_{1,E_n}^{(\text{THz,max})}]$ and the SOP equals unit as it is the integral of the PDF $f_{\gamma_{SE_n}^{(\text{THz})}}(z)$ over the whole range of $\gamma_{SE_n}^{(\text{THz})}$.

Therefore, by grouping the three above-detailed cases together, this yields (48).

C. RF link

Similarly to the FSO and THz links, the SOP of the H_n -U RF link yields from incorporating (37) with $Z = U$ and (36) with $Z = E^{(2)}$ into (42) as follows

$$P_{s,\text{Ka}}^{(2,n)} \stackrel{(a)}{=} \frac{\phi_U \phi_{E^{(2)}}}{\bar{\gamma}_{2,E^{(2)}}} \sum_{n=0}^{m_s^{(E^{(2)})} - 1} \frac{\binom{m_s^{(E^{(2)})} - 1}{n} \left(\frac{\mu_{E^{(2)}}}{\bar{\gamma}_{2,E^{(2)}}}\right)^n}{n!} \sum_{p=0}^{m_s^{(U)} - 1} \frac{\mu_U^p}{v_U^{p+1}} \times \frac{\binom{m_s^{(U)} - 1}{p}}{p!} \int_0^\infty z^n \gamma_{\text{inc}} \left(p + 1, \frac{\mu_U(2^{R_s}(1+z) - 1)}{\bar{\gamma}_{2,U}} \right) \exp\left(\frac{v_{E^{(2)}} z}{\bar{\gamma}_{2,E^{(2)}}}\right) dz, \quad (66a)$$

$$\stackrel{(b)}{=} \frac{\phi_U \phi_{E^{(2)}} \exp\left(-\frac{v_{E^{(2)}} \left[\frac{1}{2^{R_s}} - 1\right]}{\bar{\gamma}_{2,E^{(2)}}}\right)}{2^{R_s(n+1)} \bar{\gamma}_{2,E^{(2)}}} \sum_{n=0}^{m_s^{(E^{(2)})} - 1} \frac{\binom{m_s^{(E^{(2)})} - 1}{n}}{n!} \times \left(\frac{\mu_{E^{(2)}}}{\bar{\gamma}_{2,E^{(2)}}}\right)^n \sum_{p=0}^{m_s^{(U)} - 1} \frac{\binom{m_s^{(U)} - 1}{p} \mu_U^p}{v_U^{p+1}} \times \sum_{q=0}^n \frac{\binom{n}{q}}{(1 - 2^{R_s})^{q-n}} \int_{2^{R_s} - 1}^\infty \frac{\exp\left(-\frac{v_{E^{(2)}} t}{\bar{\gamma}_{2,E^{(2)}} 2^{R_s}}\right)}{t^{-q}} \left[1 - e^{-\frac{\mu_U t}{\bar{\gamma}_{2,U}}} \sum_{k=0}^p \frac{\left(\frac{\mu_U t}{\bar{\gamma}_{2,U}}\right)^k}{k!}\right] dt, \quad (66b)$$

where Step (b) can be achieved from Step (a) by virtue of the change of variable $t = 2^{R_s}(1+z) - 1$ the binomial expansion for the term $(t+1 - 2^R)^n$, and the identity [36, Eq. (8.352.1)]. Finally, using [36, Eq. (3.381.3)], (49) is reached.

REFERENCES

- [1] K. Merashad, H. Dahrouj, H. Sarrideen, B. Shihada, T. Al-Naffouri, and M.-S. Alouini, "Cloud-enabled high-altitude platform systems: Challenges and opportunities," *Frontiers in Communications and Networks*, vol. 2, p. 30, 2021. [Online]. Available: <https://www.frontiersin.org/article/10.3389/frcmn.2021.716265>
- [2] G. Karabulut Kurt *et al.*, "A vision and framework for the high altitude platform station (HAPS) networks of the future," *IEEE Commun. Surveys Tuts*, vol. 23, no. 2, pp. 729–779, Secondquarter 2021.
- [3] E. Illi, F. El Bouanani, F. Ayoub, and M.-S. Alouini, "A PHY layer security analysis of a hybrid high throughput satellite with an optical feeder link," *IEEE Open J. Commun. Soc.*, vol. 1, pp. 713–731, 2020.
- [4] I. Akyildiz *et al.*, "Terahertz band communication: An old problem revisited and research directions for the next decade," *IEEE Trans. Commun.*, vol. 70, no. 6, pp. 4250–4285, 2022.
- [5] F. J. Lopez-Martinez, G. Gomez, and J. M. Garrido-Balsells, "Physical-layer security in free-space optical communications," *IEEE Photonics J.*, vol. 7, no. 2, pp. 1–14, 2015.
- [6] P. V. Trinh, A. Carrasco-Casado, A. T. Pham, and M. Toyoshima, "Secrecy analysis of FSO systems considering misalignments and eavesdropper's location," *IEEE Trans. Commun.*, vol. 68, no. 12, pp. 7810–7823, 2020.

- [7] I. Ahmad, K. D. Nguyen, and N. Letzepis, "Performance analysis of high throughput satellite systems with optical feeder links," in *2017 IEEE Global Commun. Conf. (GLOBECOM 2017)*, Dec 2017, pp. 1–7.
- [8] E. Zedini, A. Kammoun, and M.-S. Alouini, "Performance of multibeam very high throughput satellite systems based on FSO feeder links with HPA nonlinearity," *IEEE Trans. Wireless Commun.*, vol. 19, no. 9, pp. 5908–5923, Sep. 2020.
- [9] J. Liang, A. U. Chaudhry, E. Erdogan, H. Yanikomeroglu, G. K. Kurt, P. Hu, K. Ahmed, and S. Martel, "Free-space optical (FSO) satellite networks performance analysis: Transmission power, latency, and outage probability," *IEEE Open J. Veh. Technol.*, pp. 1–18, 2023.
- [10] J. Kokkonen, J. M. Jornet, V. Petrov, Y. Koucheryavy, and M. Juntti, "Channel modeling and performance analysis of airplane-satellite terahertz band communications," *IEEE Trans. Veh. Technol.*, vol. 70, no. 3, pp. 2047–2061, Mar. 2021.
- [11] E. Erdogan *et al.*, "Site diversity in downlink optical satellite networks through ground station selection," *IEEE Access*, vol. 9, pp. 31179–31190, 2021.
- [12] R. Samy, H.-C. Yang, T. Rakia, and M.-S. Alouini, "Space-air-ground fso networks for high-throughput satellite communications," *IEEE Communications Magazine*, vol. 60, no. 12, pp. 82–87, 2022.
- [13] S. R. S. Sharma, N. Vishwakarma, and A. S. Madhukumar, "Haps-based relaying for integrated space-air-ground networks with hybrid fso/rf communication: A performance analysis," *IEEE Trans. Aerosp. Electron. Syst.*, vol. 57, no. 3, pp. 1581–1599, Jun. 2021.
- [14] O. B. Yahia, E. Erdogan, G. K. Kurt, I. Altunbas, and H. Yanikomeroglu, "HAPS selection for hybrid RF/FSO satellite networks," *Trans. Aerosp. Electron. Syst.*, vol. 58, no. 4, pp. 2855–2867, Aug. 2022.
- [15] Y. Ma, T. Lv, G. Pan, Y. Chen, and M.-S. Alouini, "On secure uplink transmission in hybrid RF-FSO cooperative satellite-aerial-terrestrial networks," *IEEE Transactions on Communications*, vol. 70, no. 12, pp. 8244–8257, Dec. 2022.
- [16] O. B. Yahia, E. Erdogan, G. K. Kurt, I. Altunbas, and H. Yanikomeroglu, "Physical layer security framework for optical non-terrestrial networks," in *2021 28th Int. Conf. Telecom. (ICT)*, 2021, pp. 162–166.
- [17] O. B. Yahia, E. Erdogan, and G. K. Kurt, "On the use of HAPS to increase secrecy performance in satellite networks," in *Proc. 2021 IEEE Int. Conf. Commun. Wkshps (ICC Workshops)*, 2021, pp. 1–6.
- [18] F. Zhou, X. Li, M. Alazab, R. H. Jhaveri, and K. Guo, "Secrecy performance for RIS-based integrated satellite vehicle networks with a UAV relay and MRC eavesdropping," *IEEE Trans. Intell. Veh.*, vol. 8, no. 2, pp. 1676–1685, 2023.
- [19] O. B. Yahia, E. Erdogan, G. K. Kurt, I. Altunbas, and H. Yanikomeroglu, "Optical satellite eavesdropping," *IEEE Trans. Veh. Technol.*, vol. 71, no. 9, pp. 10126–10131, 2022.
- [20] E. Erdogan, O. B. Yahia, G. K. Kurt, and H. Yanikomeroglu, "Optical HAPS eavesdropping in vertical heterogeneous networks," *IEEE Open J. Veh. Technol.*, vol. 4, pp. 208–216, 2023.
- [21] M. Bouabdellah and F. E. Bouanani, "A PHY layer security of a jamming-based underlay cognitive satellite-terrestrial network," *IEEE Trans. Cogn. Commun. Netw.*, vol. 7, no. 4, pp. 1266–1279, Dec. 2021.
- [22] J. Yuan, G. Chen, M. Wen, R. Tafazolli, and E. Panayirci, "Secure transmission for THz-empowered RIS-assisted non-terrestrial networks," *IEEE Trans. Veh. Technol.*, vol. 72, no. 5, pp. 5989–6000, May 2023.
- [23] K. O. Odeyemi and P. A. Owolawi, "A mixed fso/rf integrated satellite-high altitude platform relaying networks for multiple terrestrial users with presence of eavesdropper: A secrecy performance," *Photonics*, vol. 9, no. 1, 2022. [Online]. Available: <https://www.mdpi.com/2304-6732/9/1/32>
- [24] T. H. Carbonneau and D. R. Wisely, "Opportunities and challenges for optical wireless: the competitive advantage of free space telecommunications links in today's crowded marketplace," in *Wireless Technologies and Systems: Millimeter-Wave and Optical*, P. Christopher, L. Langston, and G. S. Mecherle, Eds., vol. 3232. SPIE, 1998, pp. 119 – 128.
- [25] ITU, "Prediction methods required for the design of earth-space systems operating between 20 THz and 375 THz," Recommendation, Tech. Rep. ITU-R p.1622-1, Aug. 2022.
- [26] —, "Technical and operational characteristics of satellites operating in the range 20-375 thz," Recommendation, Tech. Rep. ITU-R s.1590, Sep. 2002.
- [27] F. Nadeem, V. Kvicera, M. S. Awan, E. Leitgeb, S. S. Muhammad, and G. Kandus, "Weather effects on hybrid FSO/RF communication link," *IEEE J. Sel. Areas Commun.*, vol. 27, no. 9, pp. 1687–1697, 2009.
- [28] M. Alzenad, M. Z. Shakir, H. Yanikomeroglu, and M.-S. Alouini, "FSO-based vertical backhaul/fronthaul framework for 5G+ wireless networks," *IEEE Commun. Mag.*, vol. 56, no. 1, pp. 218–224, 2018.

- [29] ITU, "Specific attenuation model for rain for use in prediction methods," Recommendation, Tech. Rep. ITU-R p. 838-3, Mar. 2005.
- [30] —, "Attenuation due to clouds and fog," Recommendation, Tech. Rep. ITU-R p.840-7, Dec. 2017.
- [31] A. A. Farid and S. Hranilovic, "Outage capacity optimization for free-space optical links with pointing errors," *J. Lightwa. Technol.*, vol. 25, no. 7, pp. 1702–1710, July 2007.
- [32] L. C. Andrews and R. L. Phillips, *Laser Beam Propagation through Random Media: Second Edition*. Bellingham, Washington, USA: SPIE Press, 2005.
- [33] I. W. Research, *Mathematica Edition: version 13.1*. Champaign, Illinois: Wolfram Research, Inc., 2022.
- [34] I. S. Ansari, F. Yilmaz, and M.-S. Alouini, "Performance analysis of free-space optical links over Málaga (M) turbulence channels with pointing errors," *IEEE Trans. Wireless Commun.*, vol. 15, no. 1, pp. 91–102, 2016.
- [35] A. Abdi, W. Lau, M.-S. Alouini, and M. Kaveh, "A new simple model for land mobile satellite channels: first- and second-order statistics," *IEEE Trans. Wireless Commun.*, vol. 2, no. 3, pp. 519–528, 2003.
- [36] I. S. Gradshteyn and I. M. Ryzhik, *Table of Integrals, Series, and Products: Seventh Edition*. Burlington, MA: Elsevier, 2007.
- [37] A. D. Wyner, "The wire-tap channel," *The Bell System Technical Journal*, vol. 54, no. 8, pp. 1355–1387, Oct. 1975.
- [38] E. Illi, F. El Bouanani, D. B. da Costa, P. C. Sofotasios, F. Ayoub, K. Mezher, and S. Muhaidat, "Physical layer security of a dual-hop regenerative mixed RF/UOW system," *IEEE Trans. Sustain. Comput.*, vol. 6, no. 1, pp. 90–104, 2021.
- [39] N. T. Hai and S. B. Yakubovich, *The Double Mellin-Barnes Type Integrals and their Applications to Convolution Theory*. P O Box 128, Farrer Road, Singapore 9128: World Scientific Publishing Co. Pte. Ltd, 1992.
- [40] ITU, "Attenuation by atmospheric gases and related effects," Recommendation, Tech. Rep. ITU-R p.676-13, Aug. 2022.